research articles Journal of proteome research

Metabonomic Studies of Human Hepatocellular Carcinoma Using High-Resolution Magic-Angle Spinning ^{1}H NMR Spectroscopy in Conjunction with Multivariate Data Analysis

Yongxia Yang,[†,‡] Chenglong Li,[⊥,§] Xiu Nie,[∥] Xiansong Feng,[⊥] Wenxue Chen,[†,‡] Yong Yue,[†] Huiru Tang,[*,†] and Feng Deng[*,†]

State Key Laboratory of Magnetic Resonance and Atomic and Molecular Physics, Wuhan Centre for Magnetic Resonance, Wuhan Institute of Physics and Mathematics, the Chinese Academy of Sciences, Wuhan 430071, P. R. China, Graduate University of the Chinese Academy of Sciences, Beijing 100049, P.R. China, Department of General Surgery, Union Hospital, Huazhong University of Science and Technology, Wuhan 430022, P. R. China, Department of General Surgery, Wuxi No.2 People's Hospital, Jiangsu 214002, P. R. China, and Department of Pathology, Union Hospital, Huazhong University of Science and Technology, Wuhan 430022, P.R. China

Received February 2, 2007

High-resolution magic-angle spinning (MAS) ^{1}H nuclear magnetic resonance spectroscopy has been employed to characterize the metabolite composition (i.e., metabonome) of the human hepatocellular carcinoma (HCC) tumor in combination with principal component analysis (PCA). The results showed that (a) the metabonomes of both low-grade HCC and high-grade HCC tumors differ markedly from that of the adjacent non-involved tissues; and (b) low-grade HCC tumors have clear differences in metabonome from that of the high-grade HCC tumors. Compared with the non-involved adjacent liver tissues, HCC tumors had elevated levels of lactate, glutamate, glutamine, glycine, leucine, alanine, choline metabolites, and phosphorylethanolamine (PE), but declined levels of triglycerides, glucose, and glycogen. The levels of lactate, amino acids including glutamate, glutamine, glycine, leucine and alanine, choline and phosphorylethanolamine (PE) were higher but the levels of PC, GPC, triglycerides, glucose, and glycogen were lower in high-grade HCC than in low-grade HCC tumors. Compared with non-cirrhotic, low-grade HCC tumors, the cirrhotic, low-grade HCC tumors showed statistically significant increases in lactate, phosphocholine (PC), and glycerophosphocholine (GPC). The necrosis in HCC tumors resulted in a drastic increase in the levels of observable triglycerides, signals of which dominated their ^{1}H NMR spectra. These results indicated that HRMAS combined with PCA offers a useful tool for understanding the tumor biochemistry and classification of liver tumor tissues; such tool may also have some potential for liver tumor diagnosis and prognosis even when some other disease processes are present.

Keywords: Magic-angle spinning NMR • Hepatocellular carcinoma • Pattern recognition • metabonomics

Introduction

Human hepatocellular carcinoma (HCC) is the most common malignant tumor of liver representing one of the most serious human cancerous problems in the world, and its prognosis is often difficult due to its aggressiveness and lack of effective screening methods.[1] Liver cancer is more common in sub-Saharan Africa and Southeast Asia, and its incidence is generally low in South America.[1] In recent years, however, the number of people who developed liver cancer, such as HCC, is increasing throughout the world, especially in western world and Japan, probably due to chronic alcohol use and the increase of hepatitis C virus (HCV) infection.[1]

Accurate diagnosis, especially in the early stage, is essential for timely treatments and patient survival. Currently, the diagnostic imaging techniques for liver cancers include ultrasound scan (US), computer tomography (CT), fluorodexoyglucose-positron emission tomography (FDG-PET), angiography, and magnetic resonance imaging (MRI).[1] Among them, angiography is only infrequently employed in the case of vascular liver tumors due to its highly invasive nature, whereas the PET has not been proven in liver cancer and has only been used to provide help in the diagnosis of liver cancer. Ultrasound scan is inexpensive, easy to perform, and has little risk to the patient, and thus, it is often used as a screening tool. CT scan is fast and often gives more detailed image than ultrasound, though

* To whom correspondence should be addressed. E-mails: huiru.tang@wipm.ac.cn (H. R.Tang); dengf@wipm.ac.cn (F. Deng).
† Wuhan Institute of Physics and Mathematics, the Chinese Academy of Sciences.
‡ Graduate University of the Chinese Academy of Sciences.
§ Wuxi No.2 People's Hospital.
∥ Department of Pathology, Union Hospital, Huazhong University of Science and Technology.
⊥ Department of General Surgery, Union Hospital, Huazhong University of Science and Technology.

10.1021/pr070063h CCC: $37.00 © 2007 American Chemical Society

Published on Web 06/12/2007

radiation dosage is an issue and extra care has to be taken to deal with allergy to the contrast agents for some patients. CT scans are less useful in distinguishing benign tumors from the malignant tumors. MRI is an invaluable tool in helping to diagnose liver cancer and to distinguish benign from malignant tumors, although it often takes much longer time than ultrasound or CT. The "gold standard" diagnostic test for liver cancer remains a biopsy and histopathological examinations. The disadvantages of biopsy histopathology include (a) difficulties in early tumor detection and diagnosis, (b) lack of molecular information, and (c) subjectivity depending on experience of pathologist. For all aforementioned techniques, the diagnosis at the early stage is often difficult since the small tumor nodules are frequently missed, especially with US and CT techniques.[1,2] Furthermore, all these techniques provide limited or little biochemical information such as metabolite composition, which is vitally important to differentiate the pathological tissues from the non-involved ones at the molecular level.

In vivo magnetic resonance spectroscopy (MRS) is a noninvasive technique capable of locating tumor and offering some metabolic information for the abnormal tissue. For example, *in vivo* MRS has been extensively used to detect the metabolic changes of tumors in brain,[3] prostate,[4] and breast.[5] This technique has also been applied in studies of liver diseases such as chronic hepatitis,[6,7] cirrhosis,[8] and tumor.[2,9−14] *In vivo* ^{1}H MRS spectra of hepatocellular carcinoma mainly showed the signals of lipids, unresolved choline metabolites, and unresolved glutamate and glutamine.[2,9,10] From the spectra, it has been found that the ratio of total cholines (δ3.2) to CH_2 (δ1.3) of triglycerides was elevated in malignant HCC tumors,[11] and the ratios of saturated lipids (δ0.9, 1.3) to glutamate/glutamine and unsaturated olefinic lipid (δ5.3) to glutamate/glutamine were also useful for the grading of liver tumor with the unchanged levels of glutamate/glutamine.[2] *In vivo* MRS, however, is often limited by its ambiguity in metabolite assignment and quantification due to its poor spectral resolution and sensitivity.[15] *In vitro* studies conducted by combination of tissue extraction with high-resolution NMR spectroscopy offered much higher spectral resolution and sensitivity,[15−19] thus, richer metabolite information. However, the extraction procedures are complex, destructive, and may result in loss of information[20] and even further changes of metabolites. Therefore, the detailed biochemistry of HCC with respect to the normal tissues remains to be further studied *in vivo* or *ex vivo,* especially when the metabolite composition is considered as a whole.

On the basis of the combination of NMR analysis of the biological samples with multivariate data analysis, the metabonomics has become a well-established technology for metabonome analysis and found widespread applications in disease studies.[21−24] In particular, the introduction of high-resolution magic-angle spinning (HRMAS) NMR spectroscopy has made it possible to analyze the metabolite components of intact tissues *ex vivo* to avoid sample destruction.[25−36] This technique has already been used to study the metabolic characteristics of intact tissues such as brain tumor,[20] kidney carcinoma,[26] liver,[27,30,34−36] and small intestine tissues.[31] HRMAS NMR has also been used to study the chronic orotic acid induced fatty liver[27] and biochemical responses of the rat liver to toxins such as $La(NO_3)_3$[32] and α-naphthylisothiocyanate (ANIT),[33] both of which can be considered as the chemically induced liver pathologies. Furthermore, HRMAS ^{1}H NMR has been employed to characterize the donated liver-graft by studying the metabolic features of human liver biopsies in the context of organ transplantation.[37] More recently, HRMAS ^{1}H NMR was applied to the liver needle biopsies from cirrhotic, hepatitis C-affected and non-pathological tissues.[38] To our best knowledge, however, there is no HRMAS NMR study of human HCC reported yet given the importance of such pathological conditions. Such studies are expected to provide much more detailed metabolic information for HCC than that obtained from the *in vivo* MRS studies.[2,9−14]

In this paper, we report some results from the ^{1}H HRMAS NMR studies on the metabolic characteristics of low-grade and high-grade human HCC tissues in comparison with those of the adjacent non-involved tissues. Multivariate data analysis on the NMR data is used to differentiate these tissues and to reveal the metabolites attributed to such differentiation. One-way ANOVA *t* tests are also carried out on some specific metabolites and their ratios to assess the statistical significance of the metabolic changes. The overall objectives of this study are (a) to explore the potential of HRMAS ^{1}H NMR spectroscopic technique for biochemical characterization of human HCC tumor, (b) to instigate methods for sample classification in terms of the HCC grading, and (c) to understand the effects of concurrent pathological factors, such as cirrhosis, on the metabolic features of HCC.

Methods and Materials

Collection of Specimens. All tissue samples were dissected from specimens for clinical pathology evaluations, and this study was reviewed and approved by the Ethics Committee of Tongji Medical School, Huazhong University of Science and Technology. In total, 31 tissue samples were obtained from 17 living patients aged 18−77 years at the Department of General Surgery, Union Hospital, Huazhong University of Science and Technology. The HCC samples included 6 low-grade (grade I−II) and 11 high-grade (grade III−IV) HCC tumors from 17 patients. The adjacent non-involved tissue samples were from 14 of these patients and used as negative controls. The samples were snap-frozen in liquid nitrogen and then stored in a −80 °C freezer. One part of a sample was used for NMR spectroscopy analysis, and the nearest part to that was fixed in 10% formalin for pathological examination. The sample information is tabulated in Table 1.

Histopathological Examinations. All the HCC and adjacent non-involved tissues were fixed in 10% buffered formalin and then embedded in paraffin wax. Sections with a thickness of 5 μm obtained with a microtome were stained with the routine hemeatoxylin and eosin (H&E) method for assessment by Department of Pathology, Union Hospital, Huazhong University of Science and Technology. Normally, 2−5 slices were examined for each sample. HCC tumor samples were graded according to the World Health Organization (WHO) classification criteria (1990). For simplicity in this study, the grade I−II HCC tumors were assigned to low-grade, whereas the grade III−IV ones were assigned to high-grade HCC. The adjacent non-involved tissues in general had well-reserved hepatocyte shape and structure and were considered as non-pathological samples.

***Ex Vivo* HRMAS and *in Vitro* Tissue Extracts ^{1}H NMR Spectroscopy.** All the HRMAS ^{1}H NMR spectra were recorded at 300K on a Varian INOVA-600 spectrometer equipped with a Varian Nanoprobe. Tissue samples (15−25 mg) were washed with sufficient D_2O to remove blood and provide field-lock signal for NMR examination, and each sample was then placed

Table 1. Data for the HCC Samples Studied in This Work[a]

patient no.	histopathological diagnosis of HCC	grade	sex/age (year)	serum AFP (ng/mL)
1	Heteromorphic HCC and necrosis	II	M/18	13542.3
2	HCC (chordo trabecula type)	II	M/32	(-)
3	HCC (chordo trabecula type) and part of normal hepatocyte	II	M/20	12838.8
4	Differentiated HCC with tubercle cirrhosis	I	M/48	(-)
5	HCC with Portal cirrhosis and fibrosis	I	M/50	910.6
6	Differentiated HCC with Portal cirrhosis	II	F/36	(-)
7	Moderately differentiated HCC	III	M/51	ND
8	Undifferentiated HCC (with chronic schistosomiasis)	III	M/55	23.3
9	Undifferentiated HCC	IV	M/43	>25000
10	Undifferentiated HCC	IV	M/54	4263.8
11	Moderately differentiated HCC with moderate fibrosis	III	M/38	ND
12	Undifferentiated HCC with Portal cirrhosis	IV	M/58	37891.6
13	Undifferentiated HCC with Portal cirrhosis and severe necrosis	IV	F/48	623
14	Moderately differentiated HCC with Portal cirrhosis and rich fibrosis	III	M/30	3580.5
15	HCC (gland alveolus type) with Portal cirrhosis	III	F/77	25.6
16	Poorly differentiated HCC with Portal cirrhosis and rich fibrosis	III	M/44	57.6
17	Undifferentiated HCC with Portal cirrhosis	III	F/38	550.4

[a] Abbreviations: HCC, Hepatocellular carcinoma; ND, not determined. The roman numbers denote tumor grading. The serum AFP value (-) represents AFP-negative.

in a 4 mm ZrO_2 rotor with a spin rate of 2200 Hz. For all samples, a standard one-dimensional ^{1}H NMR spectrum was acquired to obtain all observable metabolite signals using one-dimensional version of NOESY pulse sequence known as NOESYPR1D in the following text (recycle delay-90-t_1-90-t_m-90-acquisition), where the t_1 delay was 3 μs and the mixing time, t_m, was 100 ms; a T_2-edited spectrum was also acquired to record the signals of small metabolites selectively using a water-presaturated standard one-dimensional Carr-Purcell-Meiboom-Gill (CPMG) pulse sequence (recycle delay-90-(τ-180-τ)$_n$-acquisition).[39] In both cases, a weak irradiation equivalent to 80 Hz was applied to suppress water signal during recycle delay of 2.5 s and mixing time, t_m, in the case of the NOESYPR1D experiment. The 90° pulse length, varying from 4.9 to 5.3 μs, was adjusted for each sample individually, and 128 transients over a spectral width of 10 kHz were collected into 32k data points. In the CPMG experiment, the relaxation time ($2n\tau$) was 360 ms. The free-induction decays (FIDs) so obtained were multiplied by an exponential function with a line-broadening factor of 0.3 Hz prior to Fourier transformation. For resonance assignment purpose, ^{1}H-^{1}H TOCSY 2D NMR spectra were also acquired for some samples with the mixing time of 50 ms, 2k data points, and 16 transients for each of the 256 increments.

To obtain the ^{1}H NMR spectrum of tissue extract, one liver tissue was pulverized in a liquid nitrogen-cooled mortar with 12% perchloric acid and centrifuged at 12 000 rpm for 20 min. Following neutralization to pH = 7 with 1 M KOH, the supernatant was centrifuged at 12 000 rpm for 10 min to eliminate $KClO_4$ precipitate and then lyophilized. For NMR measurements, the lyophilized sample was redissolved in 0.6 mL of D_2O (99.8%D, Wuhan BoPu Ltd, Chinese Academy of Sciences). ^{1}H NMR spectrum of this sample was acquired using a water-presaturated single pulse sequence with 128 transients over a spectral width of 10 kHz and 32k data points. All the spectra were phase- and baseline-corrected manually using software XWINNMR 2.1 (Bruker-Biospin, Germany). Chemical shift was referenced to the methyl group of lactate at δ1.33.

Data Reduction for HRMAS ^{1}H NMR Data and Principal Component Analysis. Water suppressed NMR spectra were bucketed and automatically integrated with a self-developed automation routine in XWINNMR. The integrals of these buckets covered the region δ 0.5−5.5 and were input as variables for principal component analysis (PCA). The region of δ 4.68−5.16 was discarded to eliminate the effect of water suppression. The aromatic regions, though containing some useful signals such as those of tyrosine, have been excluded in the PC analysis due to presence of the spinning sidebands resulting from the spinning rate restriction to about 2 kHz when the Nanoprobe was used. Consequently, the spectra over the range δ 0.5−4.68 and δ 5.16−5.5 were selected, and reduced to 226 regions each 0.02 ppm wide. Prior to pattern recognition analysis, each integral region was normalized to the sum of all integral regions for each spectrum. Principal Components Analysis (PCA) was carried out on all NMR spectra of this cohort using mean-centered scaling with the software Simca-P 10.0 (Umetrics, Sweden). Data were visualized with the PC scores plots, where each point represents an individual spectrum of a sample, and loadings plots, where each point represents a single NMR spectral region or chemical shifts. From the score and loading plots, classification of samples and the biochemical components responsible for the classification, respectively, can be shown.

Results and Discussion

Histopathological Evaluation. Table 1 shows the pathological data of patients studied here together with their serum α-fetoprotein (AFP) data. Among 17 tissues, six HCC tissues were low-grade (I−II), and the remaining 11 samples were high-grade (III−IV). Clinically, one screening test is required for the patients with liver cirrhosis to determine the serum AFP levels.[1] In general, HCC is implicated in the cirrhotic patients with liver lesions when the serum AFP levels are higher than 400−500 ng/mL.[1] However, in the 17 patients studied here, 3 patients are AFP-negative and 3 patients have serum AFP levels well below 400 ng/mL, indicating that the AFP test alone has limited values for HCC diagnosis though it may have some potential for HCC prognosis.[1] Figure 1 shows the histopathological evaluation results for adjacent non-involved, low-grade, high-grade HCC samples and one high-grade HCC with necrosis (from patient 13). The adjacent non-involved tissues showed well-reserved hepatocyte structure and shapes, whereas the HCC tissues showed irregular arrangement of cell structure with enlarged nuclei occupying more cytoplasm and nuclei were

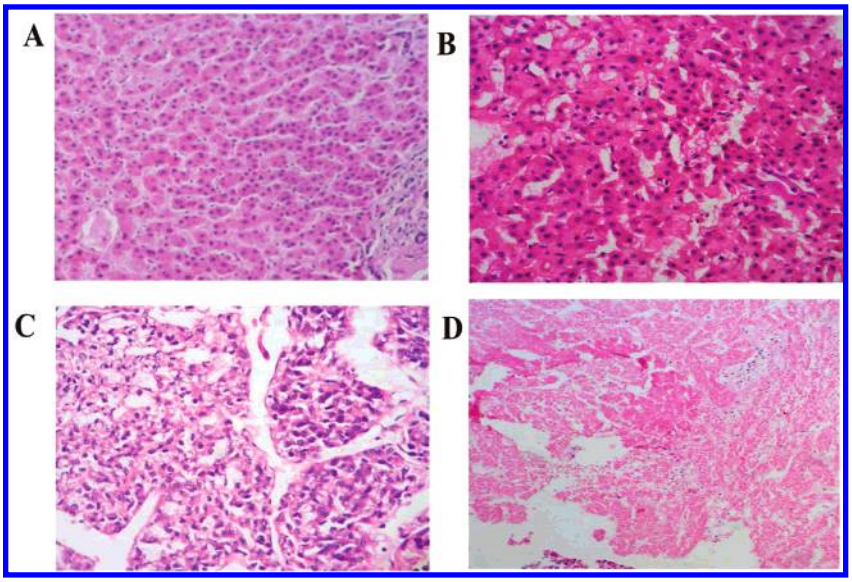

Figure 1. Haematoxylin- and eosin-stained sections of liver tissue with the magnification of 100 for (A) adjacent non-involved tissue; (B) low-grade HCC (grade I); (C) high-grade HCC (grade IV); (D) HCC form patient 13 (necrosis).

strongly eosinphilic. The HCC sample from patient 13 showed necrosis with complete loss of cell architecture. The changes in the morphological levels are expected to be accompanied with observable changes in the tissue biochemical composition which can be accessed with HRMAS ^{1}H NMR spectroscopy *ex vivo*.

HRMAS ^{1}H NMR Spectroscopy of HCC and Adjacent Non-Involved Liver Tissues. Figure 2 shows HRMAS ^{1}H NMR spectra of a grade III HCC tumor (Figure 2A,C) and an adjacent non-involved liver tissue (Figure 2B,D) from the same patient. It is clear that the spectral resolution of HRMAS NMR is comparable to the ^{1}H NMR spectrum of extract (Figure 2E). For example, the line-width of alanine peak at δ1.48 is about 2 Hz in both HRMAS CPMG (Figure 2D) and *in vitro* spectra (Figure 2E). However, the HRMAS ^{1}H NMR spectrum contains signals from lipids (e.g., δ 0.9, 1.3, 2.02, 2.25, 2.78, and 5.33) which are not in the extract spectrum. Furthermore, the tissue extract clearly showed an extra peak at δ2.41 corresponding to succinate, which is not visible in the tissue spectra. The glycogen signal at δ5.41 was also greatly enhanced in extract though it is not known whether such acidic extraction resulted in hydrolysis or not. This indicates that biochemical changes might have occurred during the tissue extraction process. Compared with *in vivo* MRS spectra,[2,9−11] HRMAS NMR spectra here contain much richer molecular information on the biochemical composition with higher resolution. For example, apart from lipids, total cholines, and unresolved glutamate and glutamine observed in the *in vivo* MRS spectra, these HRMAS NMR spectra showed signals from many other metabolites, such as valine, leucine, alanine, glycine, lactate, creatine, bile acid, phosphoethanolamine (PE), glucose, and glycogen. The resolved signals are also observed for phosphocholine (PC), glycerophosphocholine (GPC), glutamate, and glutamine.

Two types of HRMAS NMR spectra were recorded for each tissue sample, namely, NOESYPR1D (Figure 2A,B) and CPMG spectra (Figure 2C,D). The spectral signals were assigned (Table 2) based on the literature[30,32,33,38] and confirmed with ^{1}H-^{1}H TOCSY 2D NMR spectra (data not shown). The signals of lipids are dominant in the NOESYPR1D spectra (Figure 2A,B) including those at δ 0.9, 1.3, 1.59, 2.02, 2.25, 2.78, and 5.33 with the signals of the small metabolites overshadowed to some degree, though some signals of low-molecular metabolites are still visible such as creatine, leucine, valine, alanine, glycine, glutamine, and glutamate. A small signal of bile acid at δ0.73 (see expansion of Figure 2A,B) is also visible assigned to the C18 methyl resonance. The HCC tumor has a greater bile acid (δ0.73) signal probably due to bile duct obstruction common in liver impairments. This is explained by the fact that when HCC cells invade the bile duct and propagate, the bile duct may be obstructed to some extent depending on the severity, reducing the transfer of bile acid to intestine and the feed back from intestine. In comparison, lipid signals in CPMG spectra (Figure 2C,D) were attenuated to large extent due to T_2 relaxation, and the sharp signals from the small metabolites were enhanced such as those from glutamate (δ2.04), glutamine (δ2.15), choline (δ4.07), and lactate (δ1.33). The lipid signal from the CH_3 group (δ0.9) has less attenuation than the other lipid signals due to its greater mobility and longer T_2, being consistent with the previous results.[27]

Figure 3 shows the average HRMAS ^{1}H NMR spectra of all adjacent non-involved liver tissue, low-grade and high-grade HCC tissues, and the HCC samples with necrosis. Visual inspection on the spectra showed clear differences between HCC tumor and adjacent non-involved tissue. HCC tissues had higher levels of glutamate and glutamine, which was not observed in the *in vivo* MRS studies, together with the lower levels of glucose and glycogen. Compared with the adjacent non-involved tissues, the membrane phospholipid metabolites were also elevated in the HCC tissues including phosphoethanolamine (PE), phosphocholine (PC), and glycerophosphocholine (GPC). Moreover, abnormally high levels of lipid signals (Figure 3D) are dominant in the ^{1}H NMR spectra of the necrotic HCC tissues.

To obtain statistically meaningful observations for the whole spectra or metabonome, a number of samples for each group have to be analyzed as a whole. This together with the complexity of the spectra makes it extremely difficult to obtain the holistic analysis with visual inspection alone and classical statistical assessments; multivariate data analysis-based pattern recognition is more useful.

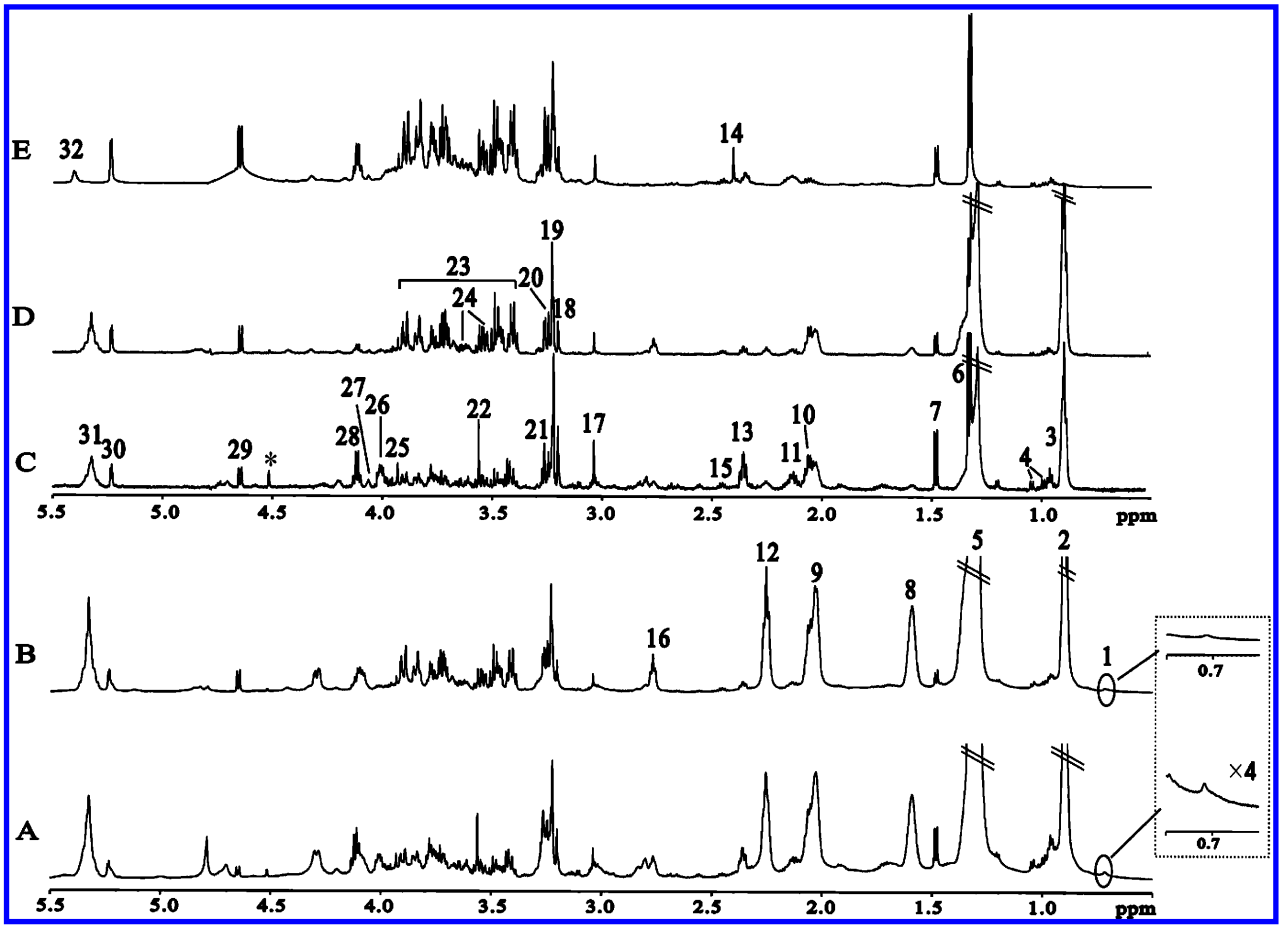

Figure 2. Representative HRMAS ^{1}H NMR spectra of HCC tumors (A and C) and adjacent non-involved tissue (B and D) from the same patient. (A and B) HRMAS NOESYPR1D spectra; (C and D) HRMAS water-suppressed CPMG spectra; (E) *in vitro* spectrum from the extracts of an adjacent non-involved tissue; asterisk, spinning sidebands.

Principal Component Analysis. In NOESYPR1D spectra, generally, signals from small metabolites such as those of amino acids are, to some extent, overlapped with resonances of lipids, whereas CPMG spectra emphasize the small metabolites but contain lipid signals as well. To emphasize the contribution of the small metabolites, PCA was first done on the CPMG spectral data. Two HCC tumor samples (from patients 1 and 13) were clear outliers, and inspection of their NMR spectra revealed abnormally high levels of lipids, implying possible occurrence of necrosis. Histopathological re-evaluation confirmed them as necrosis; hence, these two spectra were discarded from further PC analysis.

Figure 4 shows the PCA results as score and loading plots for the first two principal components from the CPMG spectra of the three groups, namely, adjacent non-involved liver tissue (○), low-grade HCC (*), and the high-grade HCC (■). The clustering is observable, respectively, for the adjacent tissues and low-grade HCC tumors, and PC1 and PC2 explained 87.7% of the total variances within the data (Figure 4A1, PC1 vs PC2, R^2 = 87.7%). The loadings plot (Figure 4A2) showed that, compared to adjacent non-involved tissues, the low-grade HCC tumors had higher levels of lactate, leucine, glutamate, glutamine, TMAO, PC/GPC, and PE but lower levels of lipids, glucose, and glycogen. One of the low-grade HCC samples (from patient 3, labeled by arrow) appeared clustering closer to the adjacent tissue. Further pathological analysis showed that there were some normal hepatocytes present in part of this sample. There was also one adjacent non-involved tissue (from patient 12, labeled by arrow) clustered closer to the low-grade HCC samples. Its NMR spectrum did have some similarities to those from low-grade HCC samples by showing higher levels of PC/GPC and lower level of glucose/glycogen even though histopathological result was not able to confirm HCC. There are two probable reasons for such discrepancy. NMR spectra and histopathology report information and changes at different levels; the former detects metabolic changes, whereas the latter observes morphological changes. It is conceivable that metabolic changes occur prior to the changes in the morphological levels. Therefore, NMR spectra may have detected some changes in the early stage which has not yet caused morphology alterations. It cannot be ruled out that some differences are present in the specimens used for NMR analysis and histopathological evaluation. The scores plot also showed clear clustered separation for the high-grade HCC tumors and adjacent non-involved tissues in PC2 (Figure 4B1). Loadings plot showed that the differences were highlighted by higher level of lactate, leucine, alanine, glutamate, glutamine, glycine, PC, GPC, and PE in high-grade HCC tumors compared with adjacent tissues (Figure 4B2).

The elevation of PE level is consistent with what was reported from a study of the rat hepatic tumors,[40] and the changes of choline metabolites are also in good agreement with previously reported results in *in vivo* MRS studies of both human HCC tumors[11,14] and rat models.[2,9,10,13] The elevation of PE and choline metabolites in HCC tumors probably resulted from metabolism of the membrane phospholipids due to accelerated

Table 2. ^{1}H NMR Data for HCC Tumor and Adjacent Non-Involved Liver Tissue[a]

metabolite	group	^{1}H chemical shift (ppm)	no.
Bile acid	C18 CH_3	0.73	1
Triglyceride	CH_3	0.90	2
	$(CH_2)_n$	1.30	5
	CH_2*-CH_2-CO	1.59	8
	CH=CH−CH_2*	2.02	9
	CH_2-CH_2*-CO	2.25	12
	CH=CH−CH_2*-CH=CH-	2.78	16
	CH*=$CHCH_2$	5.33	31
Lactate	CH_3	1.33	6
	CH	4.13	28
Leucine	δCH_3	0.94	3
Valine	γCH_3	0.98, 1.04	4
Alanine	βCH_3	1.48	7
Glutamate	βCH_2	2.04	10
	γCH_2	2.36	13
Glutamine	βCH_2	2.15	11
	γCH_2	2.45	15
Succinate	$\alpha,\beta CH_2$	2.41	14
Glycine	CH_2	3.57	22
Creatine	$N(CH_3)$	3.03	17
	$N(CH_3)_2$	3.93	25
Choline	$N^+(CH_3)_3$	3.20	18
	$CH_2(OH)$	4.07	27
PC+GPC	$N^+(CH_3)_3$	3.22	19
Trimethylamine-*N*-oxide	$N(CH_3)_3$	3.27	21
Phosphoethanolamine	OCH_2	4.01	26
β-glucose	H_2	3.24	20
	H_1	4.65	29
Glucose+Glycogen	H_{2-6}	3.50−4.00	23
Glycerol	1,3-CH_2(OH)	3.55, 3.63	24
α-glucose	H_1	5.22	30
glycogen	C1H	5.41	32

[a] Abbreviations: PC, phosphocholine; GPC, glycerophosphocholine.

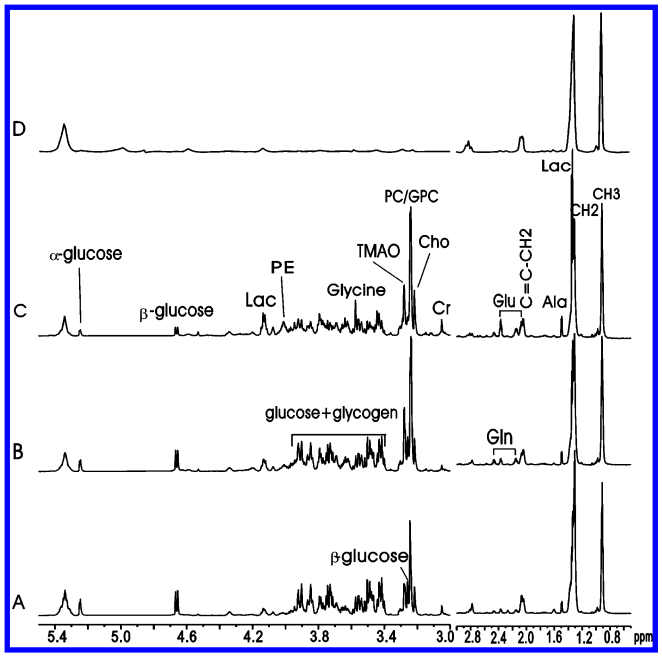

Figure 3. Average spectra from ^{1}H HRMAS CPMG experiment for (A) adjacent non-involved tissue, (B) low-grade HCC tumor, (C) high-grade HCC tumor, and (D) HCC tumors with necrosis.

cell proliferation, being consistent with the elevation of the total cholines in malignant tumors[17,18,20] and liver lesions.[32,33] Such event may also induce obstruction of bile ducts,[33] leading to the increase of bile acid signal in tumors. However, the changes of lactate, glycine, leucine, alanine, glutamate, and glutamine were not reported before in HCC tumors due to low sensitivity and resolution and probably resulted from promotion of glycolysis and disruption of TCA cycle.

Furthermore, the metabonomic differences between low-grade and high-grade HCC tissues are clearly visible (Figure 4C1). Such differences are highlighted (Figure 4C2) by the higher levels of lactate, glutamine, glutamate, alanine, leucine, creatine, PE, and glycine, and lower levels of lipids, PC/GPC, glucose, and glycogen in the high-grade HCC tumors. These metabolic differences are confirmed from the average spectra (Figure 3) of all tissues. Previous *in vivo* studies only showed that the signal ratios of saturated and unsaturated lipids to the sum of glutamine and glutamate were indicative for tumor grading,[2] where glutamine and glutamate were not resolved. In contrast, the present study showed more metabolites and their ratios which are of potential values as indicators for the HCC grading. The elevation of lactate, glutamine, glutamate, alanine, leucine, and glycine are consistent with enhanced glycolysis and effects on the TCA, whereas PE elevation is in accord with the increased membrane turnover, being reflective to the cell proliferations. However, the levels of PC/GPC and TMAO decreased to some degree in high-grade HCC tumors compared with those in low-grade HCC samples even though their signals were much higher than those in adjacent non-involved ones. The changes of PC/GPC are opposite to the PE changes in high-grade HCC tumors, and the reasons for this remain to be fully understood.

The change of glucose/glycogen metabolism has not been reported in the previous *in vivo* ^{1}H MRS studies probably also owing to its low sensitivity and spectral resolution. However, the decrease of glucose and glycogen is consistent with findings in tissue extracts in chemically induced rat models.[33] These changes are not surprising, since the anoxia conversion of glucose into lactate is fairly common in tumor cells.[41] Such depletion of glucose has also been observed in human cervical tumor.[42] Perturbations of liver metabolism by liver toxins also caused the increased rate of glycogenolysis or glycogen level reduction,[32,33] although it remains unknown whether such toxicity effects share similar molecular mechanism to that in the case of HCC development. In the present case, it is expected that the large energy requirement from the aggressive cell proliferation in HCC was the major driving force to convert glycogen to glucose, which coupled with metabolism in the TCA cycle altering the levels of the relevant metabolites.

The increase of lactate was apparent with the malignancy of HCC tumor (Figure 3) but has not yet been reported for human HCC tumors probably due to its overlapping with triglycerides[11] in the MRS studies. Increase of lactate has also been observed in breast ductal carcinomas as biomarker of progression of malignancy.[43] The lactate increase is accompanied with the increase of glycine and alanine probably resulting from glycolysis in the HCC tumor. In previous HRMAS studies of intact tissue, the resonance of lactate was normally discarded for possible anaerobic degradation of glucose induced during surgery or experiment.[43] However, it is expected that comparative metabonomics in this study will, to large degree, eliminate such effects, since all samples were subjected to the similar anaerobic processes especially in the experimental time of less than 1 h.

The lipid metabolism has been a focus for many mammalian HCC studies yielding some inconsistent results. For example, an *in vivo* image-guided ^{1}H MRS study of rat hepatocarcino-

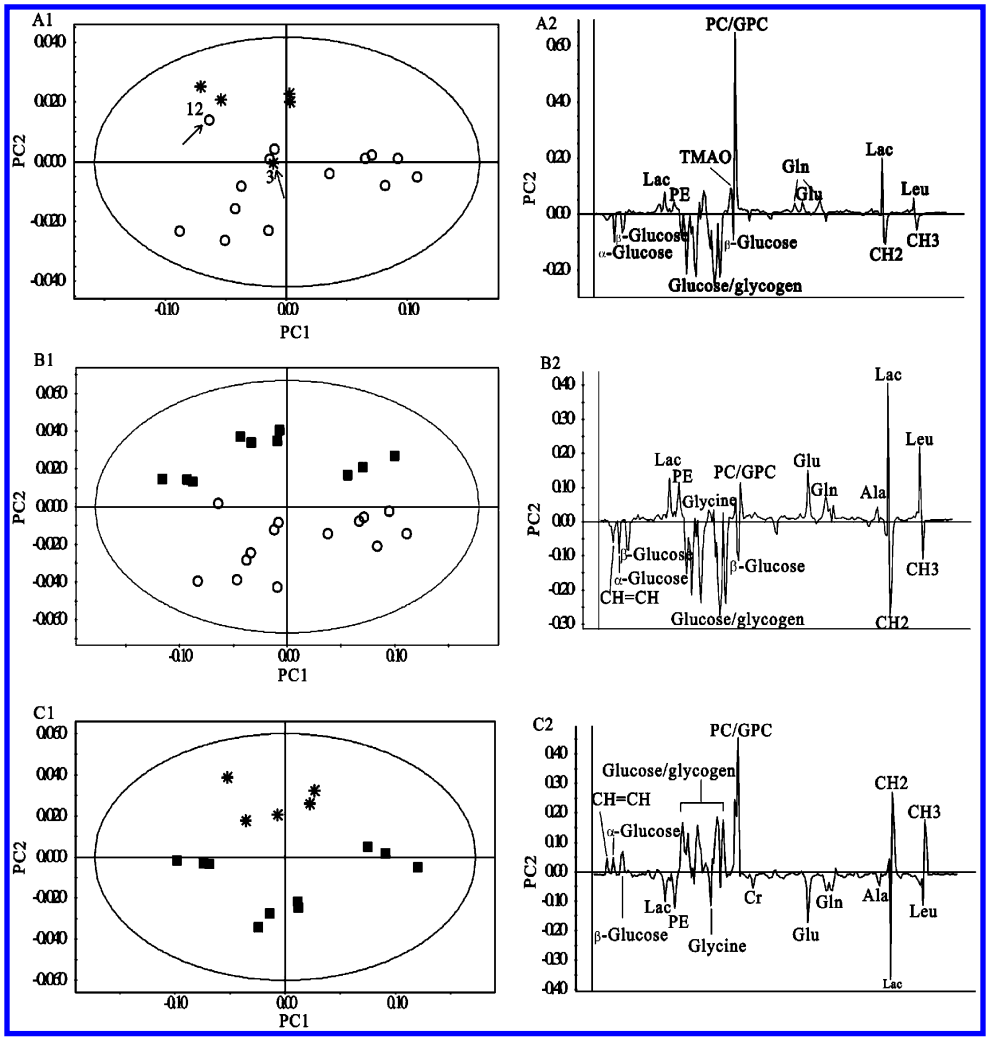

Figure 4. Principal Component Analysis to compare the metabonome of the adjacent non-involved tissue (○), low- (*), and high-grade HCC (■) based on the ^{1}H HRMAS CPMG spectra. (A1 and A2) Scores and loadings plots for adjacent non-involved tissue and low-grade HCC tumor from the PC1 and PC2 ($R^2 = 87.7\%$). Two groups were differentiated from PC2 and the metabolites with large intensities contributed to the clustering. (B1 and B2) Scores and loadings plots for adjacent non-involved tissue and high-grade HCC tumor from the PC1 and PC2 ($R^2 = 91.8\%$); two groups were separated along PC2. (C1 and C2) Scores and loadings plots for the low-grade and high-grade HCC tumors from PC1 and PC2 ($R^2 = 90\%$); two groups were separated along PC2 where the metabolites with large intensities were significant for HCC grading.

genesis model[2,9] has shown increased unsaturated olefinic lipid hydrogen at δ5.33 in HCC tumor compared to control, whereas the saturated lipid peaks at δ0.9 and δ1.3 have similar levels to the control. However, *in vivo* ^{1}H MRS study of diethyl nitrosamine (DEN)-induced HCC rats[10] showed significant decrease for the saturated lipid peaks (δ0.9 and 1.3). Such discrepancy may be originated from some differences in the pathological models and different HCC development stages.[10] In this study, nevertheless, the level of triglycerides showed clear decrease in the human HCC tumors compared with the adjacent tissues. Such decrease probably also resulted from glyconeogenesis-related conversion from triglycerides caused by the energy requirements for aggressive proliferation.

Both glutamate and glutamine are implicated in the metabonomics differences between human HCC tumors and adjacent non-involved tissues. This is in contrast with the findings in an *in vivo* MRS study of rat HCC,[2] where no changes of the levels of glutamine and glutamate were observed. This is probably due to severe overlapping between glutamine/glutamate and lipid signals, poor sensitivity, and low resolution of *in vivo* MRS. The level of glycine was much higher in high-grade HCC tumors than that in adjacent non-involved tissues and low-grade HCC tumors (Figure 3), which may provide an extra indicator for the grading of HCC tumors. It is worth noting that increased glycine level was also found in brain tumors[17,44] due to the increased glycolysis. Furthermore, the creatine level in high-grade HCC tumors was elevated, being consistent with the alteration in energy metabolism. In this study, the elevation in the levels of alanine, leucine, and valine were also found in HCC samples, again implying the involvement of glycolysis.

Moreover, there appeared some clusters among adjacent tissues along PC1 dimension (Figure 4A1 and B1) coincided with similar clustering among high-grade HCC tumors in Figure 4B1 and C1. To understand this, PCA was performed for both adjacent tissues and high-grade HCC tumors (Figure 5). In both cases, the differences in the levels of triglycerides were responsible for such clustering (Figure 5A2,B2). Close inspection also revealed that for those patients with higher level lipids in their adjacent non-involved tissues the matched HCC tissues also have higher lipid level. This implies that such clustering among

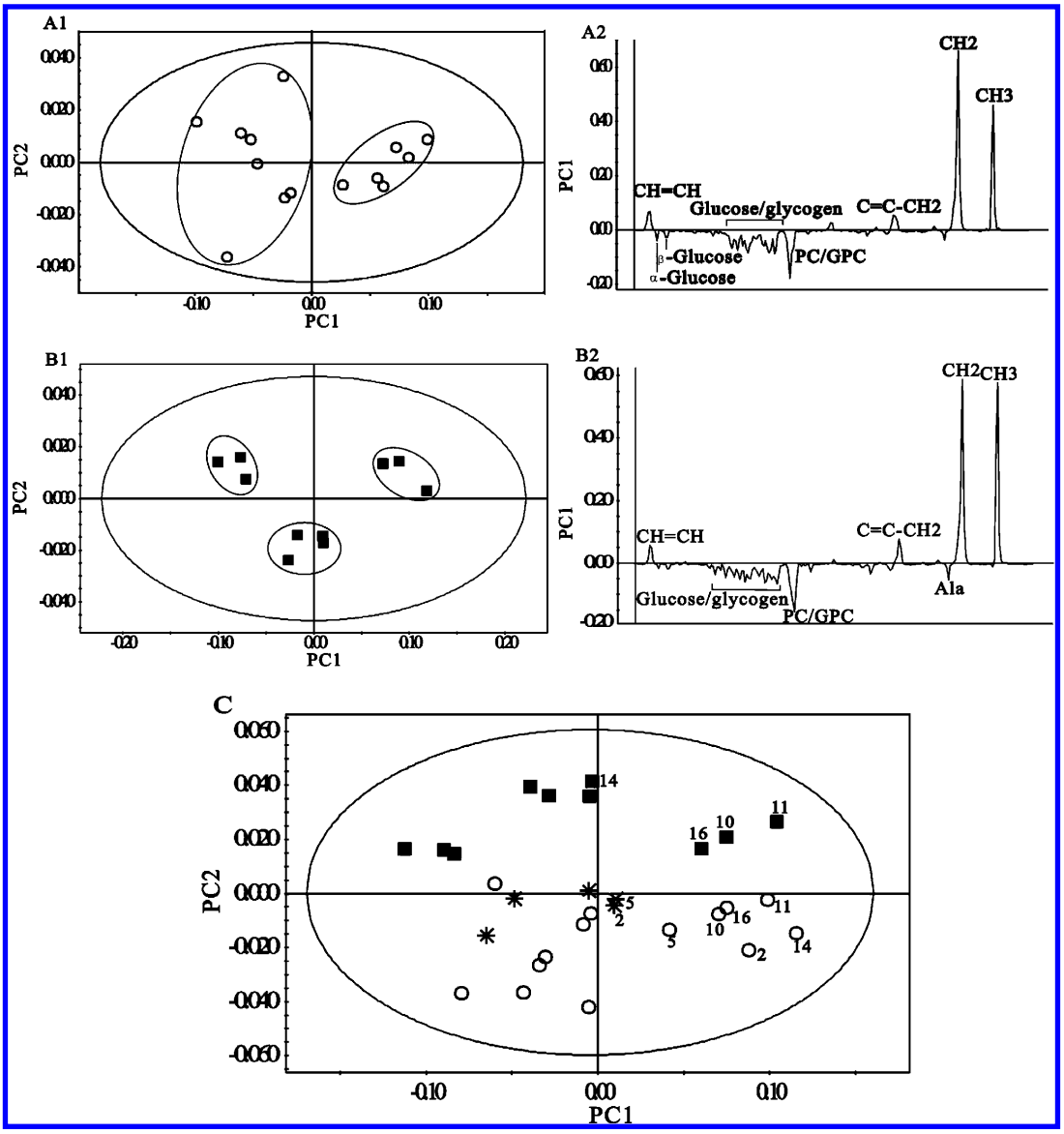

Figure 5. Results from the Principal Component Analysis for the metabonomic differences within each individual group of tissues. Panels A1 and A2 are scores and loadings plots for adjacent non-involved tissues from PC1 and PC2 (○, R^2 = 94.6%). The adjacent non-involved tissues were classified two groups along PC1 where the difference in lipid level contributed this classification demonstrating the individual diversity among samples; panels B1 and B2 are plots of high-grade HCC tissues from PC1 and PC2 (■, R^2 = 94.3%), where three clusters were observable resulting from difference in lipid level; panel C shows scores plot of all tissue specimens studied here excluding two HCC samples from patient 1 and 13, which showed severe necrosis (see text for details).

the same groups of tissues were probably due to individual differences. To ascertain this, some further studies with larger number of samples ought to be helpful. Furthermore, Figure 5 also indicated that the methods used here are useful even when the composition of the cohort is diverse and clear individual differences are present. With some follow-up studies, such individual differences are important factors to be considered, especially when the process of pathological development becomes the focus.

PC analysis was also performed on the NOESYPR1D spectra. The results were broadly in agreement with those in the above discussions, though lipid signals were by far the dominant contributing variables for sample differentiations.

Statistical Analysis. As well-known, absolute concentration quantification for metabolites is difficult in HRMAS spectroscopy, and the metabolite ratios were commonly used for statistical analysis.[45] Table 3 showed the relative signal integrals and signal ratios for some metabolites contributed to the classification of adjacent, low-grade and high-grade tissues discussed in the above sections. It is apparent that (Table 3) both glutamine and glutamate have statistical difference in high-grade HCC tumors compared with adjacent and low-grade HCC samples ($p < 0.05$) which is in contrast to the previous reports assuming their concentrations as constant. The differences in the ratios between so-called total choline (i.e., choline + PC + GPC) and the sum of glucose and glycogen have statistically significance in distinguishing the three tissue groups ($p < 0.05$, 0.15 ± 0.04, 0.25 ± 0.08, and 0.34 ± 0.11 for adjacent non-involved liver tissue, low- and high-grade HCC tumors, respectively). The ratios are also positively correlated with the grade of HCC tumors. We also calculated concentration ratios of several selected metabolites. For example, ratios of PE to β-glucose, the sum of glutamine and glutamate to glucose both have statistical difference between high-grade HCC and other

Table 3. Relative Integrals and Their Ratios from Some Selected Metabolites Contributing to the Classification of Adjacent Tissue, Low- and High-Grade HCC Tumors[a]

		non-involved	low-grade	high-grade	*p*-value
metabolites	α-glucose[&] (δ5.22)	0.73 ± 0.38	0.51 ± 0.23	0.29 ± 0.22	$0.00^{1,3}$
	β-glucose[&] (δ4.65)	1.18 ± 0.53	1.05 ± 0.49	0.47 ± 0.34	$0.00^{1,3}$
	creatine[&] (δ3.03)	0.31 ± 0.12	0.22 ± 0.12	0.53 ± 0.28	$0.01^{1,3}$, $0.01^{2,3}$
	PE[&] (δ4.01)	0.17 ± 0.15	0.68 ± 0.31	1.47 ± 0.72	$0.00^{1,3}$, $0.00^{2,3}$
	glutamine[&] (δ2.15)	0.45 ± 0.23	1.01 ± 0.58	1.63 ± 0.71	$0.00^{1,3}$, $0.02^{2,3}$
	glutamate[&] (δ2.36)	0.51 ± 0.24	0.68 ± 0.47	1.96 ± 0.96	$0.00^{1,3}$, $0.00^{2,3}$
	PC+GPC[&]δ3.22)	3.33 ± 1.63	6.08 ± 3.06	5.29 ± 3.40	$0.01^{1,3}$, $0.04^{1,2}$
metabolites ratio	tCho/(glucose+glycogen[Φ])*	0.15 ± 0.04	0.25 ± 0.08	0.34 ± 0.11	$0.00^{1,3}$, $0.03^{2,3}$, $0.02^{1,2}$
	PE/β-glucose[#]	0.16 ± 0.04	0.36 ± 0.17	1.84 ± 0.67	$0.00^{1,3}$, $0.00^{2,3}$
	Glx/β-glucose[#]	0.26 ± 0.08	0.41 ± 0.21	2.34 ± 1.02	$0.00^{1,3}$, $0.00^{2,3}$
	PE/Glx[#]	0.64 ± 0.09	1.38 ± 1.34	0.84 ± 0.23	$0.02^{1,2}$

[a] Abbreviations: Lac, lactate; PC, phosphocholine; GPC, glycerophosphocholine; Cr, creatine; PE, Phosphoryl ethanolamine; Glx, glutamate and glutamine; tCho, choline, PC, and GPC. The numbers 1, 2, and 3 denote adjacent non-involved, low-grade HCC, and high-grade HCC tissues, respectively; &, normalized integral of metabolites in spectrum (normalized to 100, chemical shift region: δ0.5−4.68 and δ5.16−5.5);*, ratios of normalized integrals; Φ, including glucose and glycogen at δ5.22 , 4.65, and δ3.5−4.0; #, concentration ratios of metabolites.

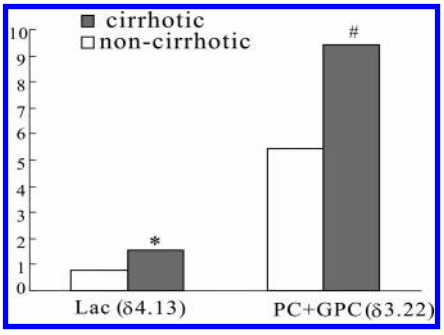

Figure 6. Histogram demonstrating the metabolic difference in non-cirrhotic and cirrhotic low-grade HCC. * $p = 0.05$; $p = 0.07$.

two groups. This indicates that metabonomic difference is probably a better tool for tumor grading than the classical individual metabolite-based targeted analysis.

Finally, since cirrhosis is one of the main risk factors for the HCC development,[1] the effect of cirrhosis on metabolism has also been assessed here. The cirrhosis led to statistically significant elevation in the levels of lactate ($p = 0.05$) and PC/GPC ($p = 0.07$) in low-grade HCC tissues (Figure 6), though changes of lipid and glycogen were found in the non-cancerous cirrhotic liver compared with normal tissue.[38] However, such statistical differences were not evident between the non-cirrhotic and cirrhotic cases in the high-grade HCC tissues probably due to the dominance of cancer cell metabolism in the high-grade HCC. Given the limited cases of cirrhotic HCC tumors at present, further studies with more samples are required to confirm these findings. Some follow-up studies on the same patients will also be important to understand the process of pathological development.

Conclusion

In summary, there are clear metabonomics differences between HCC tumor and the adjacent non-involved tissues which are highlighted by the increased levels in bile acid, choline, PE, PC, GPC, glutamate, glutamine, glycine, alanine, and leucine together with the decreased levels of lipids, glucose, and glycogen in the HCC tumors. The metabonomics approach used in this study was also able to differentiate the low-grade and high-grade HCC tumors; compared to the low-grade HCC, the levels of lactate, glutamine, glutamate, alanine, leucine, creatine, PE, and glycine were higher, while the levels of lipids, PC/GPC, glucose, and glycogen were lower in the high-grade HCC tumors. The results indicated that alteration of energy metabolism coupled with changes in TCA cycle were dominant in the HCC biochemistry. The necrosis is accompanied with drastic elevation in the lipid level. Cirrhosis caused significant increase in the levels of lactate and PC/GPC in the cirrhotic low-grade HCC tumors. With the diversity of the cohort composition, the coherency of these data showed the power and sensitivity of this metabonomic approach. It is concluded that HRMAS ^{1}H NMR spectroscopy is a powerful high-resolution tool to characterize the metabolite composition in tumors with more detailed metabolic information, which is important in the development of new diagnostic methods for HCC and perhaps in the evaluation processes of clinical therapies. Tissue metabonomics technology based on HRMAS NMR in conjunction with multivariate data analysis has an important potential in differentiating HCC from adjacent non-involved tissues and in HCC grading.

Abbreviations: Cho, choline; GPC, glycerophosphocholine; PC, phosphocholine; Gln, glutamine; Glu, glutamate; Lac, lactate; Ala, alanine; tLip, total lipid; PE, Phophorylethanolamine; Leu, leucine; TMAO, Trimethylamine-*N*-oxide.

Acknowledgment. We acknowledge the financial supports from the National Natural Science Foundation of China (20573132, 20575074, and 20425311). HRT also acknowledges financial supports from National Basic Research Program of China (2006CB503909) and the Chinese Academy of Sciences (KSCX2-YW-N-033, T012508−O5S113). We acknowledge Hanzhen Yuan and Wuyang Liu, Wuhan Institute of Physics and Mathematics, for their valuable technical assistance. We are also grateful for two anonymous referees for some excellent suggestions and comments enabling us to further improve the manuscript.

Supporting Information Available: Spectra of non-involved liver tissues and low- and high-grade HCC tumors. This material is available free of charge via the Internet at http://pubs.acs.org.

References

(1) Franca, A. V.; Elias Junior, J.; Lima, B. L.; Martinelli, A. L.; Carrilho, F. J. *Braz. J. Med. Biol. Res.* **2004**, *37*, 1689−1705.
(2) Towner, R. A.; Foley, L. M.; Painter, D. M. *Toxicol. Appl. Pharmacol.* **2005**, *207*, 237−244.
(3) Harada, M.; Tanouchi, M.; Nishitani, H.; Miyoshi, H.; Bandou, K.; Kannuki, S. *Jpn. J. Cancer Res.* **1995**, *86*, 329−332.

(4) Liney, G. P.; Turnbull, L. W.; Knowles, A. J. *NMR Biomed.* **1999**, *12*, 39−44.
(5) Jagannathan, N. R.; Singh, M.; Govindaraju, V.; Raghunathan, P.; Coshic, O.; Julka, P. K.; Rath, G. K. *NMR Biomed.* **1998**, *11*, 414−422.
(6) Cho, S. G.; Kim, M. Y.; Kim, H. J.; Kim, Y. S.; Choi, W.; Shin, S. H.; Hong, K. C.; Kim, Y. B.; Lee, J. H.; Suh, C. H. *Radiology* **2001**, *221*, 740−746.
(7) Lim, A. K.; Patel, N.; Hamilton, G.; Hajnal, J. V.; Goldin, R. D.; Taylor-Robinson, S. D. *Hepatology* **2003**, *37*, 788−794.
(8) Taylor-Robinson, S. D.; Sargentoni, J.; Bell, J. D.; Saeed, N.; Changani, K. K.; Davidson, B. R.; Rolles, K.; Burroughs, A. K.; Hodgson, H. J.; Foster, C. S.; Cox, I. J. *Liver* **1997**, *17*, 198−209.
(9) Foley, L. M.; Towner, R. A.; Painter, D. M. *Biochim. Biophys. Acta* **2001**, *1526*, 230−236.
(10) Zhao, W. D.; Guan, S.; Zhou, K. R.; Li, H.; Peng, W. J.; Tang, F.; Chen, Z. W. *J. Cancer Res. Clin. Oncol.* **2005**, *131*, 597−602.
(11) Kuo, Y. T.; Li, C. W.; Chen, C. Y.; Jao, J.; Wu, D. K.; Liu, G. C. *J. Magn. Reson. Imaging* **2004**, *19*, 598−604.
(12) Wu, B.; Peng, W. J.; Wang, P. J.; Gu, Y. J.; Li, W. T.; Zhou, L. P.; Tang, F.; Zhong, G. M. *Chin. Med. Sci. J.* **2006**, *21*, 258−264.
(13) Xu, H.; Li, X.; Yang, Z. H.; Xie, J. X. *Acad. Radiol.* **2006**, *13*, 1532−1537.
(14) Chen, C. Y.; Li, C. W.; Kuo, Y. T.; Jaw, T. S.; Wu, D. K.; Jao, J. C.; Hsu, J. S.; Liu, G. C. *Radiology* **2006**, *239*, 448−456.
(15) Usenius, J. P.; Kauppinen, R. A.; Vainio, P. A.; Hernesniemi, J. A.; Vapalahti, M. P.; Paljarvi, L. A.; Soimakallio, S. *J. Comput. Assist. Tomogr.* **1994**, *18*, 705−713.
(16) Tesiram, Y. A.; Saunders, D.; Towner, R. A. *Biochim. Biophys. Acta* **2005**, *1737*, 61−68.
(17) Peeling, J.; Sutherland, G. *Magn. Reson. Med.* **1992**, *24*, 123−136.
(18) Tosi, M. R.; Bottura, G.; Lucchi, P.; Battaglia, A.; Giorgianni, P. *J. Mol. Struct.* **2001**, *565*−*66*, 323−327.
(19) Nicholas, P. C.; Kim, D.; Crews, F. T.; Macdonald, J. M. *Anal. Biochem.* **2006**, *358*, 185−191.
(20) Cheng, L. L.; Chang, I. W.; Louis, D. N.; Gonzalez, R. G. *Cancer Res.* **1998**, *58*, 1825−1832.
(21) Brindle, J. T.; Antti, H.; Holmes, E.; Tranter, G.; Nicholson, J. K.; Bethell, H. W.; Clarke, S.; Schofield, P. M.; McKilligin, E.; Mosedale, D. E.; Grainger, D. J. *Nat. Med.* **2002**, *8*, 1439−1444.
(22) Wang, Y.; Holmes, E.; Nicholson, J. K.; Cloarec, O.; Chollet, J.; Tanner, M.; Singer, B. H.; Utzinger, J. *Proc. Natl. Acad. Sci. U.S.A.* **2004**, *101*, 12676−12681.
(23) Tsang, T. M.; Woodman, B.; McLoughlin, G. A.; Griffin, J. L.; Tabrizi, S. J.; Bates, G. P.; Holmes, E. *J. Proteome Res.* **2006**, *5*, 483−492.
(24) Martin, F. P.; Verdu, E. F.; Wang, Y.; Dumas, M. E.; Yap, I. K.; Cloarec, O.; Bergonzelli, G. E.; Corthesy-Theulaz, I.; Kochhar, S.; Holmes, E.; Lindon, J. C.; Collins, S. M.; Nicholson, J. K. *J. Proteome Res.* **2006**, *5*, 2185−2193.
(25) Cheng, L. L.; Ma, M. J.; Becerra, L.; Ptak, T.; Tracey, I.; Lackner, A.; Gonzalez, R. G. *Proc. Natl. Acad. Sci. U.S.A.* **1997**, *94*, 6408−6413.
(26) Moka, D.; Vorreuther, R.; Schicha, H.; Spraul, M.; Humpfer, E.; Lipinski, M.; Foxall, P. J.; Nicholson, J. K.; Lindon, J. C. *J. Pharm. Biomed. Anal.* **1998**, *17*, 125−132.
(27) Rooney, O. M.; Troke, J.; Nicholson, J. K.; Griffin, J. L. *Magn. Reson. Med.* **2003**, *50*, 925−930.
(28) Sitter, B.; Sonnewald, U.; Spraul, M.; Fjosne, H. E.; Gribbestad, I. S. *NMR Biomed.* **2002**, *15*, 327−337.
(29) Husted, C.; Montez, B.; Le, C.; Moscarello, M. A.; Oldfield, E. *Magn. Reson. Med.* **1993**, *29*, 168−178.
(30) Bollard, M. E.; Garrod, S.; Holmes, E.; Lindon, J. C.; Humpfer, E.; Spraul, M.; Nicholson, J. K. *Magn. Reson. Med.* **2000**, *44*, 201−207.
(31) Wang, Y.; Tang, H.; Holmes, E.; Lindon, J. C.; Turini, M. E.; Sprenger, N.; Bergonzelli, G.; Fay, L. B.; Kochhar, S.; Nicholson, J. K. *J. Proteome Res.* **2005**, *4*, 1324−1329.
(32) Wu, H.; Zhang, X.; Li, X.; Wu, Y.; Pei, F. *Anal. Biochem.* **2005**, *339*, 242−248.
(33) Waters, N. J.; Holmes, E.; Waterfield, C. J.; Farrant, R. D.; Nicholson, J. K. *Biochem. Pharmacol.* **2002**, *64*, 67−77.
(34) Yap, I. K.; Clayton, T. A.; Tang, H.; Everett, J. R.; Hanton, G.; Provost, J. P.; Le Net, J. L.; Charuel, C.; Lindon, J. C.; Nicholson, J. K. *J. Proteome Res.* **2006**, *5*, 2675−2684.
(35) Griffin, J. L.; Scott, J.; Nicholson, J. K. *J. Proteome Res.* **2007**, *6*, 54−61.
(36) Waters, N. J.; Waterfield, C. J.; Farrant, R. D.; Holmes, E.; Nicholson, J. K. *J. Proteome Res.* **2006**, *5*, 1448−1459.
(37) Vilca-Melendez, H. D.; Duarte, I. F.; Girlanda, R.; Holmes, E.; Lindon, J. C.; Gil, A. M.; Heaton, N. D.; Nicholson, J. K. *Hepatology* **2005**, *42*, 338A.
(38) Martinez-Granados, B.; Monleon, D.; Martinez-Bisbal, M. C.; Rodrigo, J. M.; del Olmo, J.; Lluch, P.; Ferrandez, A.; Marti-Bonmati, L.; Celda, B. *NMR Biomed.* **2006**, *19*, 90−100.
(39) Meiboom, S.; Gill, D. *Rev. Sci. Instrum.* **1958**, *20*, 688−691.
(40) Kobliakov, V. A.; Somova, O. G.; Kondalenko, V. F.; Ostashkina, N. M.; Kandyba, A. G.; Dubovaya, T. K.; Dyatlovitskaya, E. V. *Biochemistry (Moscow)* **2001**, *66*, 603−607.
(41) Dang, C. V.; Semenza, G. L. *Trends Biochem. Sci.* **1999**, *24*, 68−72.
(42) Sitter, B.; Bathen, T.; Hagen, B.; Arentz, C.; Skjeldestad, F. E.; Gribbestad, I. S. *Magma* **2004**, *16*, 174−181.
(43) Cheng, L. L.; Chang, I. W.; Smith, B. L.; Gonzalez, R. G. *J. Magn. Reson.* **1998**, *135*, 194−202.
(44) Lehnhardt, F. G.; Rohn, G.; Ernestus, R. I.; Grune, M.; Hoehn, M. *NMR Biomed.* **2001**, *14*, 307−317.
(45) Wang, Y.; Bollard, M. E.; Keun, H.; Antti, H.; Beckonert, O.; Ebbels, T. M.; Lindon, J. C.; Holmes, E.; Tang, H.; Nicholson, J. K. *Anal. Biochem.* **2003**, *323*, 26−32.

PR070063H